Optimal screen arrangements for a tuned liquid damper

S. Crowley & R. Porter

School of Mathematics, University of Bristol, Bristol, BS8 1TW, UK.

November 11, 2011

Abstract

Tuned Liquid Dampers (TLDs) have been installed in large engineering structures to suppress unwanted motions. They function by allowing fluid to slosh in a tank mounted rigidly to the structure which contain devices for dissipating energy. In this paper, the TLD is comprised of a rectangular tank fitted with a number of vertical slatted screens to provide damping when the fluid is in motion.

The rectangular tank TLD is coupled to a simple mechanical model for the displacement of an externally-forced structure of large mass. The influence of the fluid motion in the rectangular tank is included in this model through two components of the complex-valued net horizontal force provided by the fluid on the tank, namely the added mass and damping coefficients. These depend on both the forcing frequency and the magnitude of the tank displacement. The calculation of these key coefficients is performed by developing an analytical solution to a linearised boundary-value problem representing the forced motion of a rectangular tank having an arbitrary configuration of vertical slatted screens. The tank problem is formulated using classical water wave theory with linearised boundary conditions both on the free surface and across the screens. These latter linearised screen conditions are designed to accurately capture both the added inertia effects of a slatted screen and the damping effects from an equivalent non-linear turbulent drag law, whose successful implementation is reported in Crowley and Porter (in press). Advantage is also taken of the linearised theory used to demonstrate key qualitative features of TLD systems analytically.

Numerical results are shown to compare very well with experimental results for particular screen arrangements. Different screen configurations are then considered to indicate general criteria for 'optimising' the TLD performance, by reducing overall displacement across all forcing frequencies by altering the number, placement and porosity of the slatted screens in the tank.

1 Introduction

The suppression of unwanted large amplitude motions in large engineering structures such as bridges and tall buildings that are subject to excitation from external forces is an important part of engineering design. Typically, the inherent damping of such large structures is small and the structures will possess resonant frequencies which can be responsible for large amplitude response when excited by forcing with those frequency components. In tall

buildings, for example, vortex shedding from wind loading or earthquake-induced vibrations can supply such a forcing. Engineers mitigate against these resonances by building damping systems into the structure and tuning the damping systems to minimise motion over a range of frequencies, not just the resonant frequencies.

The forces induced by the sloshing of liquid in a tank can be utilised to damp the unwanted motions of various structures in which they are housed. So-called Tuned Liquid Dampers (TLDs) have previously been used to stabilise ships and satellites, but have most recently been employed to mitigate the dynamic response of tall buildings; Tamura *et al.* (1995) and Kareem *et al.* (1999) consider some specific examples in more detail. Such devices have been predominantly adopted by engineers in Japan, including in the Shin-Yokohama Prince Hotel and the control tower at the Narita Airport (Tamura *et al.*, 1992). Tamura *et al.* (1992) concluded that the presence of the TLD reduced the acceleration response of the tower to about 50% of that without a damper. Their study also found that after the onset of seismic excitations, the TLD significantly reduced the duration of the vibrations. TLDs have lower maintenance costs than the commonly used alternative Tuned Mass Damper (TMD) systems, their natural frequency can be easily adjusted and they can be utilised for water supply whereas a TMD has no other function. Often they can be easily retro-fitted into existing structures (e.g. Tamura *et al.*, 1995).

The more general study of liquid sloshing in tanks mounted within structures has been a subject of study over many decades, mainly motivated by the desire to suppress sloshing motions in moving containers such as oil transporters and space vehicles (see Abramson (1966), Dodge (2000) for example).

The damping that develops due to the viscosity of the fluid in the tank is usually insufficient in reducing the sloshing response (e.g. Ibrahim, 2005). Various devices are used to not only suppress the liquid sloshing response, but to also shift the natural frequencies of the liquid in the tank. Numerous studies have been conducted into the damping force in tanks of differing shapes – including rectangular, cylindrical and spherical (Abramson *et al.*, 1963) – compartmented and those fitted with screens, both solid and perforated.

A TLD works by tuning the fundamental sloshing frequency of the liquid in a tank to the natural frequency of the structure. Tanks with no added sloshing suppression systems installed rely upon violent sloshing at resonance to dissipate vibration energy, the external forces between the structure and hydrodynamic forces due to the liquid motion in the tank being transmitted through the walls of the tank. Even so, the inherent damping this provides has been found to be insufficient without extra dissipating devices installed in the tank (Fediw *et al.*, 1995; Tait and El Damatty, 2004).

Various approaches have been analysed to increase the inherent damping of the tank. Gardarsson *et al.* (2001) studied the effectiveness of a TLD with a sloped bottom. Tamura *et al.* (1992) analysed the adding of particles to the fluid on the performance of the TLD. Others have inserted devices such as screens and obstacles to dissipate the energy.

Fediw *et al.* (1995) found vertical, sharp-edged lattice screens located close to the centre of the tank to effective in increasing the inherent damping of the tank. Warnitchai and Pinkaew (1998) developed a TLD model to investigate the damping effect of three different type of flow dampening devices. In all cases the structure was placed in the middle of the tank. The wire mesh screen was found to provide significantly more damping to liquid sloshing than the vertical flat plate or two vertical circular poles. The wire mesh screen was also shown to have a negligible effect on the sloshing frequency which is important in TLD design.

Tait and El Damatty (2004) developed an equivalent mechanical model that has the same effect on the structure as a TLD. Tait *et al.* (2005) then conducted experiments to verify both linear, based on that of Fediw *et al.* (1995), and non-linear numerical models of a TLD with vertical slatted screens placed in various locations inside the tank. Investigation of the sloshing of fluid showed that if properly designed the screens were able to provide sufficient damping. Tait (2008) went on to give an equivalent linear mechanical model of a TLD that takes into account the energy dissipated by the slatted screens. This model is validated with scaled experiments, subjecting the structure-TLD system to both sinusoidal and random excitation. A preliminary procedure for designing an optimally-tuned TLD for a given structure is given.

Frandsen (2005) also considers the effectiveness of a TLD but using a fully non-linear model. However, here the TLD is modelled as a clean tank with no screens and instead the structure is given some associated damping.

Other recent work on investigating the effect of a slatted screen on sloshing in TLDs related to the current work includes that of Faltinsen and Timokha (2011). They provide an analytic solution of the natural sloshing frequencies in a rectangular tank with a centralised slat screen and show how these results depend on local properties of the screen such as the number and positioning of the slats.

Despite the previous work on TLDs, both numerical, experimental and mathematical, there appears to be little clear indication on how to systematically design an optimally-damped slatted-screen TLD device. Questions such as what shape of tank should be used, how many screens and what type of screen should be used appear to remain largely unanswered. We attempt to shed light on these issues by considering a two-dimensional rectangular tank TLD design and provide a mathematical model for the solution due to forced harmonic vibration of a structure containing a TLD.

In the first part of this paper we consider the fluid response and horizontal component of the hydrodynamic forces due to the forced motion of a rectangular tank with a single centrally-placed screen. The governing equations are based on classical linearised water wave theory, whose accuracy is questionable for large fluid responses but since we are attempting to damp optimally, we argue that it is a reasonable tool to use. Fediw *et al.* (1995) confirms this, finding that increasing the number or decreasing the porosity of the screens in the water tank results a more linear sloshing response. Indeed, recent results of Faltinsen *et al.* (2011b) indicate that linear theory matches experimental Faltinsen *et al.* (2011b) indicate that linear theory matches experimental results even for large amplitude free surface motions. Love and Tait (2010) use experimental results of structure-TLD systems subject to random forcing in order to verify proposed models. They conclude that a linear model is sufficient for preliminary TLD design. A similar theoretical basis has been used by Tait (2008) and Faltinsen *et al.* (2011a) in their related investigations.

In order to advance the mathematical solution given in section 2, we require a screen-averaged linear relationship between flux and pressure drop to provide a condition at the slatted screen. This is modelled via a complex coefficient which includes a real part associated with the added inertia (a blockage coefficient) provided by the constrictions in the screen and an imaginary part associated with damping.

Crowley and Porter (in press) describe an approach to model these two effects accurately by equating the coefficients with equivalent, more accurate, models of flow past a single slatted screen. The same approach is adopted here in determining a screen-averaged boundary condition at a number of screens along the tank.

In section 3, we show how the analysis of section 2 can be developed to deal with any number of screens in the tank showing that an exact description of the solution can be found by applying simple transfer matrices to each component of the depth dependence to produce a simple solution technique. This is similar to the approach used by Evans (1990) when considering analytically the reflection of waves by a number of vertical, equally spaced porous screens in both an open ended and closed narrow rectangular wave tank.

In section 4 a TLD design is considered by coupling the solution of section 3 for the tank sloshing to a mechanical model of the large structure. Key features of the behaviour of a TLD are demonstrated analytically by our theoretical model, such as the suppression of resonance of the structure by the tank and the development of two new resonances at frequencies above and below the original resonance. Numerical results show excellent agreement with the scale-model experiments of Tait (2008). Having verified our theoretical model, we then consider a range of TLD designs and produce numerical results showing TLD operation. For given sets of parameters, such as the tank fill ratio and the structural mass/fluid mass ratio, we investigate what are the optimal number, placement and characteristics of the screens such that the structural motion is reduced to a minimum over all excitation frequencies. The paper is summarised in section 5.

2 A horizontally-forced rectangular container with a single screen

We use Cartesian coordinates (x, y) with $y = 0$ coinciding with the undisturbed free surface of a fluid contained in a two-dimensional rectangular tank with base at $y = h$. When at rest, the sidewalls of the tank are positioned at $x = \pm a$ and a single thin vertical slatted screen extends through the depth at $x = 0$. The system is forced into horizontal oscillations of amplitude $\epsilon \ll a$ and with angular frequency ω, and we are considering the long-time behaviour of the motion (i.e. transients in an initial-value problem have died away). The screen provides damping through the production of turbulent eddies shed from the sharp edges of the slats, and the standard arguments suggest that these eddies remain largely localised to the screen on account of the oscillating fluid motion – see Mei *et al.* (1983). Then it is usual to assume the bulk flow is irrotational and inviscid whilst the fluid is taken to be incompressible. Regions close to the screen are treated separately and eventually collapsed onto the screen to form boundary conditions across the screen.

We use classical linearised water wave equations to describe the fluid motion (see the discussion in the Introduction) in which the fluid velocity is given by the gradient of a potential $\Phi(x, y, t) = \Re\{\omega\epsilon\phi(x, y)\mathrm{e}^{-\mathrm{i}\omega t}\}$. Then ϕ satisfies

$$\nabla^2\phi = 0, \qquad \text{in the fluid,} \tag{2.1}$$

$$\phi_y = 0, \qquad \text{on } y = h, \tag{2.2}$$

the linearised free surface condition

$$K\phi + \phi_y = 0, \qquad \text{on } y = 0, \tag{2.3}$$

where $K = \omega^2/g$ and g is gravitational acceleration. On the vertical walls of the tank, the horizontal velocity of the fluid is imposed by

$$\Phi_x = \omega\epsilon\cos\omega t, \qquad \text{on } x = \pm a + \epsilon\sin\omega t, \tag{2.4}$$

4

which, when linearised, is equivalent to requiring

$$\phi_x = 1, \qquad \text{on } x = \pm a, \, 0 < y < h. \tag{2.5}$$

Finally, we require conditions relating properties of the flow on one side of the screen to the other. For this, we follow the recent work of Crowley and Porter (in press) who themselves followed closely ideas of Bennett *et al.* (1992) and Mei *et al.* (1983). The effects of the local flow field in the presence of the slatted barrier are considered, initially isolating a narrow strip either side of the screen before contracting those conditions onto the line occupied by the screen thereby allowing us to formulate approximate boundary conditions on the screen.

As a result we obtain a condition expressing continuity of horizontal velocity across the screen,

$$[\phi_x]_{x=0^-}^{x=0^+} = 0, \qquad 0 < y < h, \tag{2.6}$$

where the square brackets denote the jump in the enclosed quantity.

A dynamic condition is also derived that takes into account both the non-linear turbulent drag and added inertial effects felt by the fluid as it accelerates through the constrictions of the slatted screen. Adopting the approach used in Crowley and Porter (in press) the drag and inertia effects are determined empirically from idealised mathematical models the condition is written

$$[\phi]_{x=0^-}^{x=0^+} = k^{-1}\gamma \left(\phi_x(0, y) - 1 \right), \qquad 0 < y < h, \tag{2.7}$$

the right-hand side involving the relative velocity of the fluid and the moving screen. In the above, $\gamma = \mathbb{C} + i\mathbb{K}_L$, $\mathbb{C}$ and $\mathbb{K}_L$ are, respectively the blockage and linearised drag coefficients found using the methods described in Crowley and Porter (in press) and k is defined to be the positive real root of the dispersion equation

$$K = k \tanh kh. \tag{2.8}$$

Note that whilst $\mathbb{C}$ is determined by the geometry of the screen, the depth and the wave frequency, the linearised drag coefficient, $\mathbb{K}_L$, is determined by an iterative procedure, being dependent also on free surface amplitudes either side of the screen which themselves are part of the solution. This is simply a by-product of linearising a non-linear drag law. The iterative procedure is itself not an onerous numerical task and the advantages of being able to solve a linearised hydrodynamic problem outweigh the numerical effort of iteration.

In the case being considered in this section, of a single screen centrally placed in the rectangular tank, it is clear that oscillations will be antisymmetric, implying that $\phi(-x, y) = -\phi(x, y)$ and then equations (2.1), (2.2), (2.3) and (2.5) may be solved in $x > 0$ only with (2.6) and (2.7) replaced by the single condition

$$2\phi(0^+, y) = k^{-1}\gamma \left(\phi_x(0^+, y) - 1 \right), \qquad 0 < y < h, \tag{2.9}$$

and with the relation $\phi(-x, y) = -\phi(x, y)$ providing the extension into $x < 0$.

However, with a few to developing more general configurations of multiple screens, we choose not to take advantage of this symmetry condition. Thus, we expand the potential in each subdomain $x < 0$ and $x > 0$ in terms of separation solutions, writing

$$\phi^{(j)}(x, y) = \sum_{n=0}^{\infty} \chi_n^{(j)}(x) \psi_n(y), \tag{2.10}$$

5

with

$$\chi_n^{(j)}(x) = \left(a_n^{(j)}\mathrm{e}^{-k_n x} + b_n^{(j)}\mathrm{e}^{k_n x}\right)/k_n, \tag{2.11}$$

where $j = 0$ refers to $-a < x < 0$ and $j = 1$ to $0 < x < a$. In the above, $a_n^{(j)}$ and $b_n^{(j)}$ are expansion coefficients to be determined, whilst

$$\psi_n(y) = N_n^{-1/2} \cos k_n(y - h), \qquad N_n = \frac{1}{2}\left(1 + \frac{\sin 2k_n h}{2k_n h}\right), \tag{2.12}$$

for $n \geq 0$ are vertical eigenfunctions with k_n given as the real positive roots of

$$K = -k_n \tan k_n h, \qquad n \geq 1, \tag{2.13}$$

and $k_0 \equiv -\mathrm{i}k$ where k is already defined by (2.8). The functions ψ_n satisfy the orthogonality relation

$$\frac{1}{h}\int_0^h \psi_n(y)\psi_m(y)\mathrm{d}y = \delta_{mn}, \qquad m, n \geq 0. \tag{2.14}$$

Writing

$$1 = \sum_{n=0}^{\infty} L_n \psi_n(y), \tag{2.15}$$

with

$$L_n = \frac{1}{h}\int_0^h \psi_n(y)\mathrm{d}y = \frac{N_n^{-1/2}\sin k_n h}{k_n h}, \tag{2.16}$$

it is clear that the structure of the boundary conditions (2.5), (2.6) and (2.7) with (2.15) allow us to apply these conditions separately to each Fourier mode. In other words we have

$$\chi_n^{(0)'}(-a) = \chi_n^{(1)'}(a) = L_n, \qquad \chi_n^{(0)'}(0) = \chi_n^{(1)'}(0), \tag{2.17}$$

and

$$\chi_n^{(1)}(0) - \chi_n^{(0)}(0) = k^{-1}\gamma\left(\chi_n^{(0)'}(0) - L_n\right), \tag{2.18}$$

where primes denote differentiation. Using the second condition in (2.17) and (2.18) first and substituting in from (2.11), we find that

$$\begin{pmatrix} a_n^{(0)} \\ b_n^{(0)} \end{pmatrix} = T(\lambda_n)\begin{pmatrix} a_n^{(1)} \\ b_n^{(1)} \end{pmatrix} + \lambda_n L_n \begin{pmatrix} 1 \\ 1 \end{pmatrix}, \tag{2.19}$$

where

$$T(x) = \begin{pmatrix} 1+x & -x \\ x & 1-x \end{pmatrix}, \tag{2.20}$$

is a transfer matrix, connecting modal amplitudes from one side of the screen to the other, and

$$\lambda_n = k_n \gamma/(2k). \tag{2.21}$$

Finally, applying the lateral boundary conditions (2.17) leads, after considerable algebra, to

$$\begin{pmatrix} a_n^{(1)} \\ b_n^{(1)} \end{pmatrix} = \frac{L_n}{2(\lambda_n \sinh k_n a + \cosh k_n a)}\begin{pmatrix} \lambda_n(1 - \mathrm{e}^{k_n a}) - 1 \\ \lambda_n(1 - \mathrm{e}^{-k_n a}) + 1 \end{pmatrix}, \tag{2.22}$$
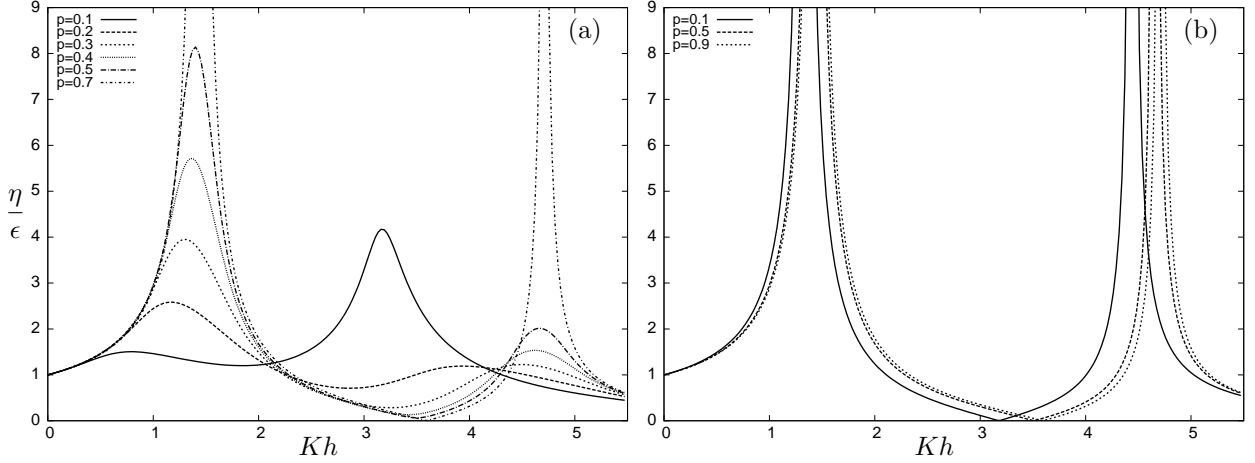
FIGURE 1: Magnitude of the free surface at the left hand wall $x = -a$, for a tank of aspect ratio $a/h = 1$ with a centered screen of varying porosity. The tank is forced to oscillate with an amplitude of $\epsilon/h = 0.01$. In (b) the screen has no damping.

and then it follows from (2.19) that

$$
\begin{pmatrix} a_n^{(0)} \\ b_n^{(0)} \end{pmatrix} = \frac{L_n}{2(\lambda_n \sinh k_n a + \cosh k_n a)} \begin{pmatrix} \lambda_n(\mathrm{e}^{-k_n a} - 1) - 1 \\ \lambda_n(\mathrm{e}^{k_n a} - 1) + 1 \end{pmatrix}. \tag{2.23}
$$

The total potential can be reconstructed using (2.11) with (2.22) and (2.23) and this gives

$$
\chi_n^{(0)}(x) = \frac{L_n(\lambda_n(\cosh k_n(x + a) - \cosh k_n x) + \sinh k_n x)}{k_n(\lambda_n \sinh k_n a + \cosh k_n a)}, \tag{2.24}
$$

whilst it can also be shown that $\chi_n^{(1)}(x) = -\chi_n^{(0)}(-x)$, as expected illustrating the potential to be antisymmetric.

Note that in the special case of $\gamma = 0$, then the solution coincides with a forced rectangular container of width $2a$ with no screen present, namely

$$
\phi(x, y) = \sum_{n=0}^{\infty} \frac{L_n \sinh k_n x \, \psi_n(y)}{k_n \cosh k_n a}, \tag{2.25}
$$

for $-a < x < a$, $0 < y < h$.

Also, when $\gamma \to \infty$, it is straightforward to confirm that the solution is equivalent to a forced rectangular container of width a (i.e. the tank is divided equally into two compartments with an impermeable wall between them) and then

$$
\phi^{(0)} = \sum_{n=0}^{\infty} \frac{L_n \sinh k_n(x + \frac{1}{2}a) \, \psi_n(y)}{k_n \cosh \frac{1}{2}k_n a}, \tag{2.26}
$$

and $\phi^{(1)}(x, y) = -\phi^{(0)}(-x, y)$.

Figure 1(a) plots the magnitude of the dimensionless free surface at the left hand wall $x = -a$ of a tank with a single centrally placed screen and tank aspect ratio $a/h = 1$. In
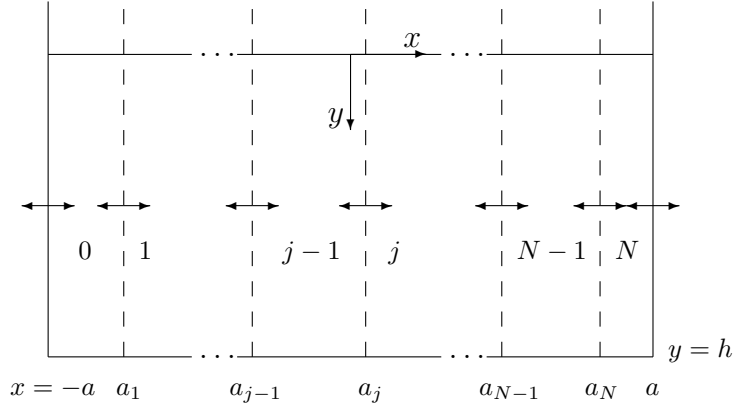
FIGURE 2: N screens inserted at $x = a_j$, $j = 1, \ldots, N$ with walls at $x = \pm a$. The labelling indicates the $N + 1$ separate regions of the tank.

agreement with (2.25) as $\gamma \to 0$ (which occurs when the screen porosity $p \to 1$) resonant behaviour is seen at the first and second sloshing frequencies associated with a tank with no screens, $ka = \frac{1}{2}\pi, \frac{3}{2}\pi$ or $Kh \approx \frac{1}{2}\pi, \frac{3}{2}\pi$ respectively. As the porosity of the screen decreases, $\gamma \to \infty$, the peaks at those frequencies vanish. However, another peak emerges relating to the natural frequency of a completely divided tank at $ka = \pi$, or $Kh \approx \pi$, as expected by (2.26).

More generally, if $\gamma = \mathbb{C}$ is real (i.e. there is no damping), then the potential is undefined at values of frequency determined by (2.8) where k satisfies $\cot ka = \frac{1}{2}\mathbb{C}$ (where $k_0 = -\mathrm{i}k$) determined from (2.24), (2.21), and these are the sloshing frequencies of the undamped tank. If there are no screens present then these occur at $k = p_m$ where $p_m = (m + \frac{1}{2})\pi/a$ for $m = 0, 1, \ldots$, as the porosity of the screen decreases (hence $\gamma = \mathbb{C}$ increases), the first sloshing frequency of the tank will decrease from these values as shown in Figure 1(b).

3   Multiple screens

We extend the previous case of one screen in the centre of the tank to N vertical screens placed at arbitrary positions $x = a_j$, $j = 1, \ldots, N$. For convenience, we extend this notation to include the two end walls by defining $a_0 = -a$ and $a_{N+1} = a$.

Within each of the separate $N + 1$ fluid-filled sections of the container, bounded by two screens $a_j < x < a_{j+1}$, the velocity potential is given $\phi = \phi^{(j)}$ as defined by (2.10) with $\chi_n^{(j)}$ a slightly modified version of (2.11) given by

$$\chi_n^{(j)}(x) = \left(a_n^{(j)}\mathrm{e}^{-k_n(x-a_j)} + b_n^{(j)}\mathrm{e}^{k_n(x-a_j)}\right)/k_n, \tag{3.1}$$

for $j = 0, \ldots, N$. For simplicity we will assume that each screen has the same porosity and gap-slat structure, although the dependence of the imaginary component of γ (the linearised drag coefficient) upon the surface wave amplitudes either side of the screen imply that different values of γ_j must now be applied to each screen in the tank. Thus the conditions across each screen are now written

$$\chi_n^{(j-1)'}(a_j) = \chi_n^{(j)'}(a_j), \qquad \text{and} \qquad \chi_n^{(j)}(a_j) - \chi_n^{(j-1)}(a_j) = k^{-1}\gamma_j\left(\chi_n^{(j)'}(a_j) - L_n\right), \tag{3.2}$$

8

for $j = 1, \ldots, N$ whilst the end wall conditions remain as

$$\chi_n^{(0)'}(a_0) = \chi_n^{(N)'}(a_{N+1}) = L_n. \tag{3.3}$$

The strategy is to successively connect solutions from one section to the next through transfer matrices, before finally applying wall conditions. Such a process is reminiscent of the wide-spacing approximation (e.g. Martin, 2006) widely applied to wave interactions between multiple scatterers where evanescent wave effects are often discarded to make simple connections between wave fields either side of a scatterer. Here, we are applying the same methodology but do so mode-by-mode and therefore make no approximation to the solution.

Thus, applying (3.2) to (3.1) for each $j = 1, \ldots, N$ gives

$$\begin{pmatrix} a_n^{(j-1)} \\ b_n^{(j-1)} \end{pmatrix} = T_n^{(j)} \begin{pmatrix} a_n^{(j)} \\ b_n^{(j)} \end{pmatrix} + \lambda_n^{(j)} L_n \begin{pmatrix} e^{k_n c_j} \\ e^{-k_n c_j} \end{pmatrix}, \tag{3.4}$$

where

$$T_n^{(j)} = \begin{pmatrix} (1 + \lambda_n^{(j)})e^{k_n c_j} & -\lambda_n^{(j)}e^{k_n c_j} \\ \lambda_n^{(j)}e^{-k_n c_j} & (1 - \lambda_n^{(j)})e^{-k_n c_j} \end{pmatrix} \equiv \Delta(k_n c_j)T(\lambda_n^{(j)}), \tag{3.5}$$

is the transfer matrix for the jth screen where T and $\lambda_n^{(j)}$ are defined by (2.20) and (2.21) with $\gamma = \gamma_j$, $c_j = a_j - a_{j-1}$ and

$$\Delta(x) = \begin{pmatrix} e^x & 0 \\ 0 & e^{-x} \end{pmatrix}, \tag{3.6}$$

embodies the 'phase shift' of a wave between adjacent screens.

Applying (3.5) recursively across all N screens gives

$$\begin{pmatrix} a_n^{(0)} \\ b_n^{(0)} \end{pmatrix} = \boldsymbol{T}_n^{(N)} \begin{pmatrix} a_n^{(N)} \\ b_n^{(N)} \end{pmatrix} + L_n \boldsymbol{F}_n \begin{pmatrix} 1 \\ 1 \end{pmatrix}, \tag{3.7}$$

where, for $j = 1, \ldots, N$,

$$\boldsymbol{T}_n^{(j)} = T_n^{(1)} T_n^{(2)} \ldots T_n^{(j)}, \tag{3.8}$$

and

$$\boldsymbol{F}_n = \sum_{j=1}^{N} \boldsymbol{T}_n^{(j)} \lambda_n^{(j)}. \tag{3.9}$$

In deriving (3.7) we have made use of the fact that

$$T_n^{(j)} \begin{pmatrix} 1 \\ 1 \end{pmatrix} = \begin{pmatrix} e^{k_n c_j} \\ e^{-k_n c_j} \end{pmatrix}. \tag{3.10}$$

Instead of relating the coefficients $a_n^{(0)}$, $b_n^{(0)}$ in terms of $a_n^{(N)}$, $b_n^{(N)}$ as given in (3.7), we could equally well have related $a_n^{(N)}$, $b_n^{(N)}$ in terms of $a_n^{(0)}$, $b_n^{(0)}$. Of course, this can be done directly by operating through (3.7) by the inverse of $\boldsymbol{T}_n^{(N)}$ and it can be shown that the two approaches give the same result.

We continue by writing

$$\boldsymbol{T}_n^{(N)} \equiv \begin{pmatrix} t_{11} & t_{12} \\ t_{21} & t_{22} \end{pmatrix} \qquad \text{and} \qquad \boldsymbol{F}_n \begin{pmatrix} 1 \\ 1 \end{pmatrix} \equiv \begin{pmatrix} f_1 \\ f_2 \end{pmatrix}. \tag{3.11}$$

9

Then it only remains to apply the wall conditions (3.3), a process which eventually gives

$$\begin{pmatrix} a_n^{(N)} \\ b_n^{(N)} \end{pmatrix} = \frac{L_n}{D} \begin{pmatrix} t_{12} - t_{22} + e^{k_n c_{N+1}}(1 - (f_2 - f_1)) \\ t_{21} - t_{11} + e^{-k_n c_{N+1}}(1 - (f_2 - f_1)) \end{pmatrix}, \tag{3.12}$$

where $D = (t_{21}-t_{11})e^{k_n c_{N+1}}+(t_{22}-t_{12})e^{-k_n c_{N+1}}$. For a single screen placed centrally in a tank of width $2a$, (3.12) can be shown to reduce to (2.22). To recover the remaining expansion coefficients for $j < N$, we simply use (3.7) and the solution is complete.

3.1   Horizontal force on the tank

The sloshing motion of the fluid exerts hydrodynamic forces on the tank expressed as $\Re\{F_t e^{-i\omega t}\}$, and we can now find these analytically using the integrated pressure $P = \Re\{p e^{-i\omega t}\}$, over all vertical surfaces including the tank walls and screens. Here, $P = -\rho\Phi_t$ so that $p = i\omega\rho\phi$ and thus the net horizontal force for N screens is

$$F_t = i\omega\rho \int_0^h \left(\phi(a_0, y) - \phi(a_{N+1}, y) + \sum_{j=1}^N [\phi(x, y)]_{x=a_j^-}^{x=a_j^+} \right) dy. \tag{3.13}$$

On account of the decomposition in (2.10) the depth dependence can be explicitly integrated to give

$$\begin{aligned} F_t &= i\omega\rho h \sum_{n=0}^\infty L_n \sum_{j=0}^N \left(\chi_n^{(j)}(a_j) - \chi_n^{(j)}(a_{j+1}) \right) \\ &= i\omega\rho h \sum_{n=0}^\infty \frac{L_n}{k_n} \sum_{j=0}^N \left(a_n^{(j)}(1 - e^{-k_n c_{j+1}}) + b_n^{(j)}(1 - e^{k_n c_{j+1}}) \right). \end{aligned} \tag{3.14}$$

It is usual practice to decompose F into its real and imaginary components by writing

$$F_t = -i\omega \left(A + \frac{iB}{\omega} \right), \tag{3.15}$$

where A is the termed the added mass and B the damping coefficient. These quantities can be non dimensionalised using $m = 2\rho a h$, the mass of water in the tank, such that

$$F_t = -i\omega m \left(\mu + i\nu \right), \qquad \text{where} \qquad \frac{A}{m} = \mu \qquad \text{and} \qquad \frac{B}{m\omega} = \nu. \tag{3.16}$$

We can also obtain an independent expression for the damping component of the force ν. With reference to figure 2, we apply Green's Identity to the potential ϕ and ϕ^* in each sub-region of the tank, where the asterisk denotes the complex conjugate. Thus,

$$\iint_V \phi^*\nabla^2\phi - \phi\nabla^2\phi^* \, dx\, dy = \int_S \phi^*\frac{\partial\phi}{\partial n} - \phi\frac{\partial\phi^*}{\partial n} \, dS, \tag{3.17}$$

where $\partial/\partial n$ is the derivative of the outward normal to the surface S bounding the volume V.

10

The left-hand side of (3.17) is clearly zero whilst evaluating the components of the line integral along the boundary S of each sub-region V, on $y = 0$ and $y = h$ the integrand is zero, and we are left with contributions along the vertical walls and screens. At $x = \pm a$, we have $\phi_x = 1$, and at each screen $x = a_j$ we have $[\phi_x]_-^+ = 0$ and $k^{-1}\gamma_j(\phi_x - 1) = [\phi]_-^+$.

Summing the contributions from each sub-region of the tank results, after considerable algebra, in

$$\sum_{j=0}^{N} \int_0^h (\phi - \phi^*)|_{x=a_j^+} \, \mathrm{d}y - \sum_{j=1}^{N+1} \int_0^h (\phi - \phi^*)|_{x=a_j^-} \, \mathrm{d}y = \sum_{j=1}^{N} \left(\frac{k}{\gamma_j} - \frac{k}{\gamma_j^*} \right) \int_0^h \left| [\phi]_{x=a_j^-}^{x=a_j^+} \right|^2 \, \mathrm{d}y. \quad (3.18)$$

The left-hand side of (3.18) is proportional to the integrated pressure over the walls (see equation (3.13)). Specifically it is $(F_t + F_t^*)/(\mathrm{i}\omega\rho)$, and so we find using (3.16) that

$$\nu = -\frac{k\rho}{m} \Im \sum_{j=1}^{N} \{\gamma_j^{-1}\} \int_0^h \left| [\phi]_{x=a_j^-}^{x=a_j^+} \right|^2 \, \mathrm{d}y. \quad (3.19)$$

This equation relates the overall tank damping to the damping over individual screens since

$$\Im\{\gamma_j^{-1}\} = -\frac{\mathbb{K}_L^{(j)}}{\mathbb{C}^2 + \mathbb{K}_L^{(j)2}}, \quad (3.20)$$

confirming that ν is non-negative and that, as the screen damping $\mathbb{K}_L^{(j)}$ for each screen tends to zero, then the overall tank damping ν tends to zero also.

Using the modal decomposition of ϕ in (2.10) and the orthogonality condition (2.14), (3.19) reduces to

$$\begin{aligned} \nu &= -\frac{kh\rho}{m} \sum_{j=1}^{N} \Im\left\{\gamma_j^{-1}\right\} \sum_{n=0}^{\infty} \left| \chi_n^{(j)}(a_j) - \chi_n^{(j-1)}(a_j) \right|^2 \\ &= -\frac{kh\rho}{m} \sum_{j=1}^{N} \Im\left\{\gamma_j^{-1}\right\} \sum_{n=0}^{\infty} \frac{|a_n^{(j)} - a_n^{(j-1)}\mathrm{e}^{-k_n c_j} + b_n^{(j)} - b_n^{(j-1)}\mathrm{e}^{k_n c_j}|^2}{|k_n|^2}, \end{aligned} \quad (3.21)$$

after (2.11) is used. This provides and alternative, independent, method for computing ν and can be used to check the numerical method.

We also note that (3.19) is essentially a conservation of energy relation, which is unsurprising given its roots in (3.17). To see this, we may calculate the mean power over a cycle exerted by the force on the tank which is simply the time-averaged product of the overall force on the tank and the enforced (unit) velocity of the tank and given by

$$W_{in} = \tfrac{1}{2}\Re\{F_t.1\} = \tfrac{1}{2}m\omega\nu, \quad (3.22)$$

from (3.16) (the dimensions of power – and previously force – are recovered by re-scaling ϕ appropriately). Conversely, the power lost over a cycle through damping at the screens is the mean rate of working of the pressure summed over each of the screens, which can be expressed as

$$\begin{aligned} W_{out} &= -\tfrac{1}{2}\Re\left\{ \sum_{j=1}^{N} \int_0^h (\phi_x - 1)\left[-\mathrm{i}\omega\rho\phi^*\right]_{x=a_j^-}^{x=a_j^+} \, \mathrm{d}y \right\} \\ &= -\frac{\omega\rho k}{2} \sum_{j=1}^{N} \Im\{\gamma_j^{-1}\} \int_0^h \left| [\phi]_{x=a_j^-}^{x=a_j^+} \right|^2 \, \mathrm{d}y = \tfrac{1}{2}m\omega\nu, \end{aligned} \quad (3.23)$$

11

after use of (2.7) applied to the screen at $x = a_j$ and (3.19). Hence, the net power lost per cycle is the same as the net input of power, as must be the case.

It helps to identify key features of sloshing and damping of multiple screens by examining the forces on a tank with no screens and with a centrally-placed screen, where solutions (see the end of section 2) are explicit.

3.1.1 Tank with no screens

Using (2.25) the total force on the walls at $x = \pm a$ can be calculated as

$$F_t = -2\mathrm{i}\omega\rho h \sum_{n=0}^{\infty} \frac{L_n^2 \tanh k_n a}{k_n}. \tag{3.24}$$

Note that in this case, a tank with no screens, there is no damping. Then $\nu = 0$ whilst

$$\mu = \sum_{n=0}^{\infty} \frac{L_n^2 \tanh k_n a}{k_n a}, \tag{3.25}$$

which is unbounded at sloshing frequencies.

3.1.2 Tank with a single central screen

For the case of one screen at $x = 0$ considered in §2, and exploiting the fact that ϕ is antisymmetric,

$$\begin{aligned}
F_t &= -2\mathrm{i}\omega\rho \int_0^h \left(\phi^{(1)}(a, y) - \phi^{(1)}(0^+, y) \right) dy \\
&= -2\mathrm{i}\omega\rho h \sum_{n=0}^{\infty} \frac{L_n^2 (2\lambda_n(\cosh k_n a - 1) + \sinh k_n a)}{k_n(\lambda_n \sinh k_n a + \cosh k_n a)}.
\end{aligned} \tag{3.26}$$

In the limit as $\gamma \equiv \gamma_1 \to 0$, $\lambda_n \equiv \lambda_n^{(1)} \to 0$ also, so the screen vanishes and (3.26) unsurprisingly coincides with (3.24), as shown in figure 3. When $|\gamma| \to \infty$, the tank is effectively divided into two separate compartments and now we find that

$$F_t \to -4\mathrm{i}\omega\rho h \sum_{n=0}^{\infty} \frac{L_n^2 \tanh \frac{1}{2} k_n a}{k_n}, \tag{3.27}$$

or, equivalently, $\nu = 0$ and

$$\mu \to 2 \sum_{n=0}^{\infty} \frac{L_n^2 \tanh \frac{1}{2} k_n a}{k_n a}, \tag{3.28}$$

twice the value as for a tank with no screen having double the width. In both case of $\gamma \to 0$ and $|\gamma| \to \infty$ zero damping occurs, demonstrating that optimal damping occurs for an intermediate value of γ, some way from zero and infinity in the complex plane.
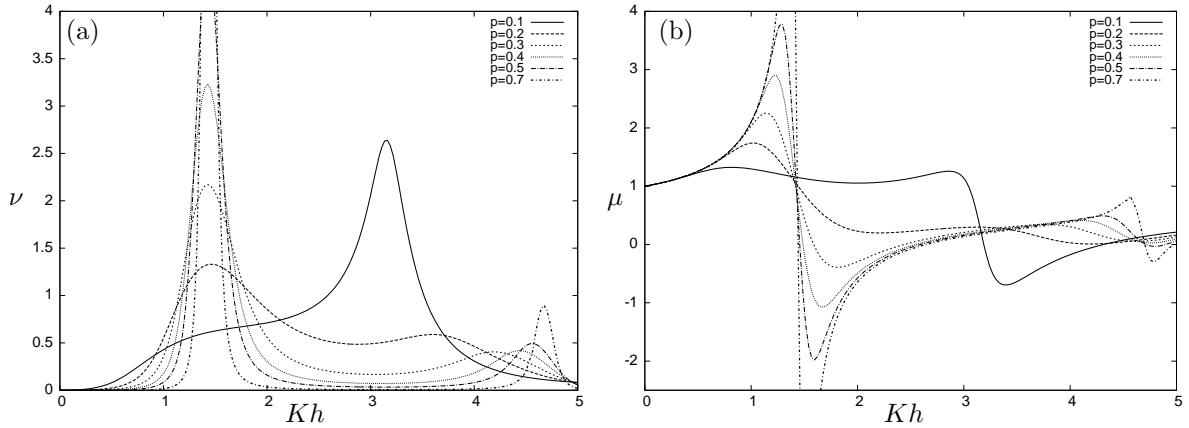
FIGURE 3: Non dimensional (a) damping and (b) added mass components of the force on the walls and screen of a tank with aspect ratio $a/h = 1$. Screen centered and of varying porosity.

3.1.3 Zero frequency limit

Consider the limit of (3.25) or (3.28) as $\omega \to 0$. Then $K \to 0$ in (2.8) and (2.13) which implies $k^2 \sim \omega^2/gh \to 0$ where $k_0 = -ik$ and $k_n h \to n\pi$ for $n \geq 1$, whilst $N_0 \to 1$ and $N_n \to \frac{1}{2}$ for $n \geq 1$. Then $L_n \to 0$ for all $n \geq 1$ and, according to either (3.25) or (3.28) for tanks with no screen or a single screen, $\mu \to 1$, as in Fig. 3(b). That is to say, the damping tends to zero and the added mass tends to the mass of water in the tank in the limit of frequency going to zero. This is entirely expected, as in the low frequency limit, the fluid acts as a solid mass moving with the tank. Though not transparent in (3.14) which gives the force for an arbitrary arrangement of screens, it is reasonable to assume that this result should also hold.

4 Coupling tank sloshing motions to an external structure

4.1 Equations of motion

The fluid-filled rectangular tank with damping screens investigated in the previous section can, when rigidly attached to a structure much larger than itself, can be used to model the effect of a so-called Tuned Liquid Damper (TLD).

The system is shown in figure 4 and consists of a structure of mass M which is subject to an external forcing $F_e(t)$, a function of time, t, and whose horizontal displacement $X(t)$ is constrained by a linear restoring spring of stiffness κ. This is an idealised mechanical model of, for example, a tall building subject to wind forces. It is typical then that $M \gg m$ where m is the mass of fluid in the attached tank and it is assumed for simplicity that no external damping mechanism is attached to the mass M.

The equation of motion for the system is given by,

$$M\ddot{X}(t) = -\kappa X + F_e(t) + F_t(t), \tag{4.1}$$

where $F_t(t)$ is the force exerted on the tank by the motion of the fluid within the tank.
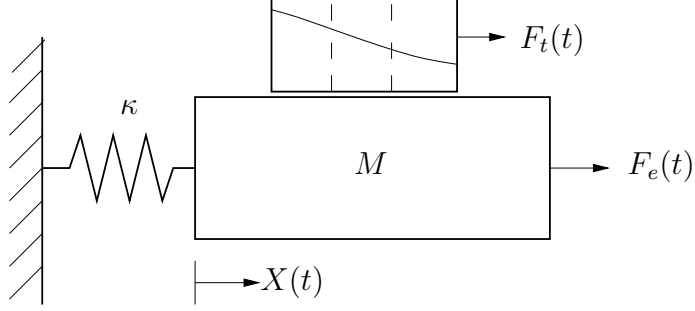
13

FIGURE 4: Structure-TLD system

It is clear that in the absence of the tank, the undamped structure is prone to resonance at a frequency given by

$$\Omega^2 = \kappa/M. \tag{4.2}$$

With the tank attached, the liquid in tank will be forced to slosh and the idea is to tune the damping characteristics, the tank geometry and both the number and placement of screens 'optimally' such that it suppresses the structure's response to the external forcing F_e. As we shall demonstrate below, damping of the structural resonance can be achieved by tuning the fundamental resonant sloshing frequency of the tank near to Ω, the natural frequency of the structure. This is the well-known principle by which both TLD's and tuned mass dampers work, although it is superficially counterintuitive. See, for example, Ibrahim (2005).

We assume that excitation is time-harmonic of angular frequency ω, and then the response of the structure and the TLD will be time-harmonic also and we write

$$F_{e,t}(t) = \Re\{f_{e,t}\mathrm{e}^{-\mathrm{i}\omega t}\}, \qquad X(t) = \Re\{x\mathrm{e}^{-\mathrm{i}\omega t}\}. \tag{4.3}$$

The force supplied by the tank f_t is proportional to the velocity of motion $(-\mathrm{i}\omega x)$ and can written

$$F_t = \omega^2 \left(A + \frac{\mathrm{i}B}{\omega} \right) x, \tag{4.4}$$

in terms of A is the added mass and B the damping coefficient, previously calculated in section 3 for a tank moving with unit velocity.

Therefore the frequency-dependent equation of motion (4.1) becomes,

$$\left(M\omega^2 + \omega^2 \left(A + \frac{\mathrm{i}B}{\omega} \right) - \kappa \right) x = -f_e. \tag{4.5}$$

Using the non-dimensionalisation of A and B in (3.16), we rearrange the above to give a non-dimensional response

$$\hat{x} \equiv \left| \frac{x}{f_e/(M\Omega^2)} \right| = \frac{\Omega^2/\omega^2}{|1 + \hat{m}(\mu + \mathrm{i}\nu) - \Omega^2/\omega^2|}, \tag{4.6}$$

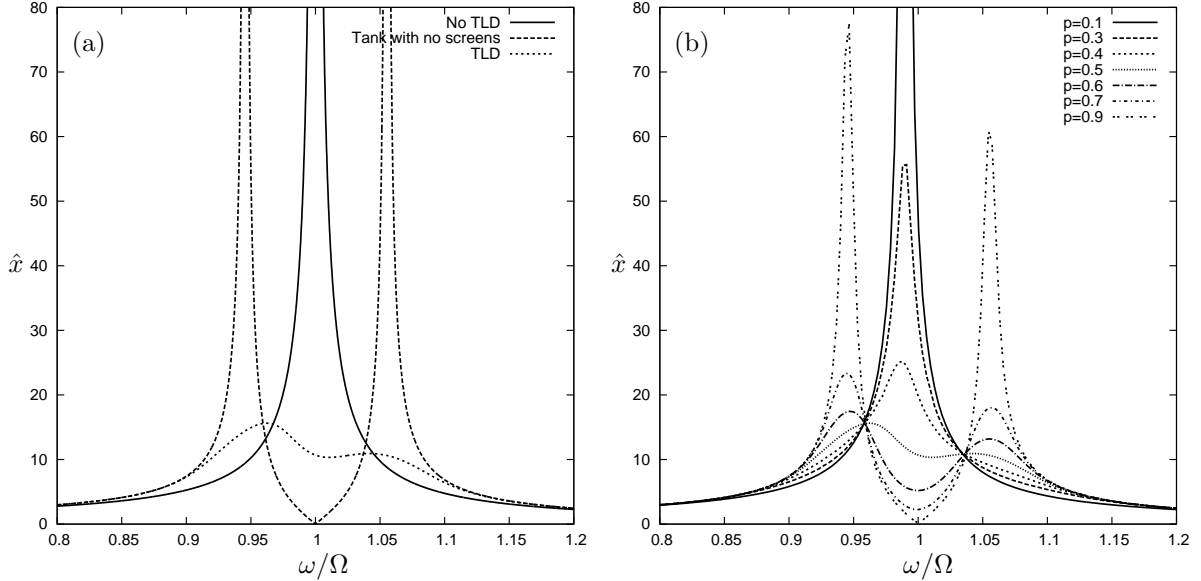where $\hat{m} = m/M$ and Ω is defined by (4.2).

14

FIGURE 5: In (a), we show a comparison of the non dimensional displacement of a structure with the addition of a tank with no screens and with a TLD consisting of a tank of aspect ratio $a/h = 3$ fitted with a single centrally placed screen of porosity $p = 0.5$. In (b), the porosity of a centered screen in a TLD with $a/h = 3$ is varied to show the effect on the displacement of the structure.

4.2 Analysis of resonance

We first demonstrate that, for a tank with no screens and hence no damping, that the structural resonance is suppressed simply by the presence of the tank. First, if no tank is attached, then $\hat{m} = 0$ and (4.6) gives

$$\hat{x} = \frac{\Omega^2}{|\omega^2 - \Omega^2|}, \tag{4.7}$$

and $\hat{x}$ is unbounded as $\omega \to \Omega$, tends to unity for $\omega \to 0$ and to zero as $\omega \to \infty$.

For a tank with no screen, $\nu = 0$ and μ is given by (3.25). The form of (3.25) does not highlight the precise nature of resonance and so we re-approach the problem for forced sloshing of an empty tank using a different method. Hence we define $\phi = \psi + x$ where ψ is now harmonic in $-a < x < a$, $0 < y < h$ and satisfies homogeneous conditions on the tank walls

$$\psi_x = 0, \qquad \text{on } x = \pm a, \qquad \psi_y = 0, \qquad \text{on } y = h, \tag{4.8}$$

with an inhomogeneous condition on the free surface,

$$\psi_y + K\psi = Kx, \qquad \text{on } y = 0. \tag{4.9}$$

The problem for ψ can be solved by separating variables and finding eigenvalues associated with the x-variable. Thus it is not difficult to show that

$$\phi(x,y) = x - 2K \sum_{n=0}^{\infty} \frac{(-1)^n \sin p_n x \cosh p_n(y-h)}{p_n^2 a(K \cosh p_n h - p_n \sinh p_n h)}, \tag{4.10}$$

15

where $p_n = (n + \frac{1}{2})\pi/a$. Defining ω_n to be the natural sloshing frequencies of an empty tank with $\omega_n^2/g = p_n \tanh p_n h$, and $K = \omega^2/g$ as usual, (4.10) can be written

$$\phi(x, y) = x - \frac{2\omega^2}{a} \sum_{n=0}^{\infty} \frac{(-1)^n \sin p_n x \cosh p_n(y - h)}{p_n^2(\omega^2 - \omega_n^2) \cosh p_n h}. \tag{4.11}$$

The force exerted by the fluid on the tank is

$$F = \mathrm{i}\omega\rho \int_0^h (\phi(-a, y) - \phi(a, y))\,\mathrm{d}y = -\mathrm{i}\omega\left[m - \frac{4\rho\omega^2}{ag} \sum_{n=0}^{\infty} \frac{\omega_n^2}{p_n^4(\omega^2 - \omega_n^2)}\right], \tag{4.12}$$

where $m = 2\rho ah$ is the mass of the fluid. In other words, the non-dimensional added mass is

$$\mu = 1 - \frac{2\omega^2}{a^2 gh} \sum_{n=0}^{\infty} \frac{\omega_n^2}{p_n^4(\omega^2 - \omega_n^2)}, \tag{4.13}$$

with $\nu = 0$ and $\mu \to 1$ as $\omega \to 0$ as already observed in §3. Now we see from (4.13) that as $\omega \to \omega_0$, say, that

$$\mu \sim \alpha - \frac{\beta\omega^2}{\omega^2 - \omega_0^2}, \qquad \text{for } \omega \text{ close to } \omega_0, \tag{4.14}$$

where the values of α and β (positive) can be identified from (4.13) but are not significant.

Substituting (4.14) into (4.6) we find

$$\hat{x} \sim \frac{\Omega^2 |\omega^2 - \omega_0^2|}{|((1 + \hat{m}\alpha)\omega^2 - \Omega^2)(\omega^2 - \omega_0^2) - \beta\hat{m}\omega^4|}. \tag{4.15}$$

Hence, $\hat{x} = 0$ when $\omega = \omega_0$ and, in particular, we can choose a tank configuration for which the fundamental sloshing frequency $\omega_0 = \Omega$, the resonance frequency of the structure and then a system previously exhibiting an infinite resonance is now completely at rest at that frequency, by the addition of the tank of fluid.

However this process introduces two new frequencies at which the structure may exhibit infinite resonance and these occur at zeros of the denominator of (4.15) or when ω is one of the positive solutions of the equation

$$(1 + \hat{m}(\alpha - \beta))\omega^4 - (\Omega^2 + \omega_0^2(1 + \hat{m}\alpha))\omega^2 + \Omega^2\omega_0^2 = 0. \tag{4.16}$$

If, as suggested, we set $\omega_0 = \Omega$, then solutions of this equation are given by

$$\omega^2 = \Omega^2 \left(\frac{1 + \frac{1}{2}\hat{m}\alpha \pm (\hat{m}\beta + \frac{1}{4}\hat{m}^2\alpha^2)^{1/2}}{1 + \hat{m}(\alpha - \beta)}\right). \tag{4.17}$$

This shows that a pair of new resonances occur in close proximity to the original resonance. Assuming that $\hat{m} \ll 1$, we estimate these values as $\omega^2/\Omega^2 = 1 + \frac{1}{2}\hat{m}(\beta - \alpha) \pm \sqrt{\hat{m}\beta} + O(\hat{m}^{3/2})$ occurring at values above and below unity with a lower order offset. This effect can be observed in figure 5(a). For this configuration, values for α and β calculated from (4.13) predict resonances at $\omega/\Omega \approx \sqrt{0.998 \pm 0.109}$.

Consider now a tank with a small amount of damping. Thus, we may think of a tank with a single centrally-placed screen for simplicity and, as before focus, on the fundamental frequency. In the absence of the screen, the fundamental resonant frequency ω_0 is defined

TLD Configuration	a/h	a (m)	h (m)	$\hat{m}$
T2	2	0.674	0.337	0.045
T3	3	0.494	0.165	0.016
T4	4	0.384	0.096	0.007

TABLE 1: Chosen TLD configurations: dimensions and mass ratios.

by $\omega_n^2/g = p_n \tanh p_n h$ with $n = 0$ where now p_n satisfies the relation $\cot p_n a = 0$ defining $p_n = (n + \frac{1}{2})\pi/a$. This corresponds to a singularity in the force at $\omega = \omega_0$. In the presence of the screen, the end of §2 showed that the condition for resonance, or a pole in the complex force $\mu + i\nu$, for a single screen is replaced by $\cot p_n a = \frac{1}{2}\gamma$, $\gamma = \mathbb{C} + i\mathbb{K}_L$. This relation defines complex p_n and hence complex ω_n. If the screen is highly porous, so that the blockage and damping effects are small (characterised by a parameter $\epsilon \ll 1$) the fundamental resonant frequency moves into the complex plane from $\omega = \omega_0$ to $\omega = \omega_0 + \frac{1}{2}\epsilon(\omega_r - i\omega_i)$, say where $\omega_i > 0$ for reasons of causality. Detailed values attributed to quantities such as ω_r, ω_i, in terms of values of $\mathbb{C}$ and $\mathbb{K}_L$, have been omitted for clarity. Appealing to the ideas of analytic continuation and referring to (4.14) in which the screen was absent, we may now assume a complex force of the form

$$\mu + i\nu \sim \alpha - \frac{\beta\omega^2}{\omega^2 - (\omega_0 + \frac{1}{2}\epsilon(\omega_r - i\omega_i))^2}, \qquad \text{for } \omega \text{ close to } \omega_0, \qquad (4.18)$$

where $\alpha = \alpha_r + i\epsilon\alpha_i$ and $\beta = \beta_r + i\epsilon\beta_i$ now to include a small imaginary component. The added mass μ and damping ν are then of the form

$$
\begin{aligned}
\mu(\omega) &\sim \alpha_r - \frac{\beta_r \omega^2(\omega^2 - \omega_0^2 - \epsilon\omega_0\omega_r)}{(\omega^2 - \omega_0^2 - \epsilon\omega_0\omega_r)^2 + \epsilon^2\omega_0^2\omega_i^2}, \\
\nu(\omega) &\sim \frac{\beta_r \epsilon\omega^2\omega_i(\omega_0 + \frac{1}{2}\epsilon\omega_r) - \beta_i \epsilon\omega^2(\omega^2 - \omega_0^2 - \epsilon\omega_0\omega_r)}{(\omega^2 - \omega_0^2 - \epsilon\omega_0\omega_r)^2 + \epsilon^2\omega_0^2\omega_i^2},
\end{aligned}
\qquad (4.19)
$$

for ω close to ω_0. The added mass clearly now varies rapidly about a mean value of $\mu = \alpha_r$ as ω^2 varies about $\omega_0^2 + \epsilon\omega_0\omega_r$ whilst ν reaches a peak value of $\beta_r\omega_0/(\epsilon\omega_i) + \frac{3}{2}\beta_r\omega_r/\omega_i$ when $\omega^2 = \omega_0^2 + \epsilon\omega_0\omega_r$. From the form taken for μ in (4.19) it can be shown that μ takes local minimum/maximum values at $\omega^2 = \omega_0^2 + \epsilon\omega_0\omega_r \pm \epsilon\omega_0\omega_i + O(\epsilon^2)$ and that the jump in μ from minimum to maximum is $\beta_r\omega_0/(\epsilon\omega_i)$, the same at the leading order peak value of the damping. This is a well-known phenomenon first described by Kramers and Krönig, (e.g. Kronig, 1926) and we illustrate these features in Figure 3.

Assuming the tank configuration is chosen such that the fundamental sloshing frequency is tuned to $\omega_0 = \Omega$, the displacement at $\omega = \omega_0$ can be found from (4.6) using (4.19) and one finds that

$$\hat{x} = \frac{1}{\hat{m}\,|\mu(\omega_0) + i\nu(\omega_0)|} \approx \frac{\epsilon(\omega_r^2 + \omega_i^2)^{1/2}}{\hat{m}\beta_r\omega_0}, \qquad (4.20)$$

to leading order in ϵ. This now implies a finite value of the displacement $\hat{x}$ at what was resonance with no tank and zero displacement with a tank in the absence of damping. Note also that though ϵ is assumed small, having the small quantity $\hat{m}$ in the denominator implies an amplification of $\hat{x}$ at this point.

17

Screen configuration	Number of screens	Screen locations
A	1	0
B	2	$\pm 0.2a$
C	2	$\pm 0.7a$
D	3	$\pm 0.5a$, 0
E	4	$\pm 0.2a$, $\pm 0.6a$

Table 2: Initial test screen configurations: number and locations

The pair of infinite resonances in the undamped tank, at frequencies determined by the vanishing of (4.15) become large finite resonances in the presence of damping, due to the complex expression that replaces the denominator of (4.15) once the assumed form (4.18) is used in (4.6). A prolonged calculation whose details are suppressed here shows that the height of these resonances is approximated by $\hat{x} \sim O(1/\epsilon)$.

The presence of screens in the tank provides a damping force that will reduce the un-wanted oscillations of the structure under excitation at the natural frequency of the structure. With no tank, the structure has a resonant frequency Ω at which its response $x \to \infty$. A tank with no screens damps out the structure's response completely at Ω, but creates two new resonances either side. A tank with one or more screens if tuned optimally will minimise the structure's response across a range of frequencies.

4.3 Numerical Procedure

The dimensionless response of the TLD structure subject to time-harmonic forcing of angular frequency ω is given by the seemingly straightforward equation (4.6). However, as highlighted earlier in §2, the linearised drag coefficient used for determining the solution is, according to the approach developed by Crowley and Porter (in press), a function of the free surface wave amplitudes incident either side of each screen in the tank. Thus, for any given $\hat{x}$ which can be mapped onto values of ϵ, an iterative root-finding procedure must be undertaken to find linearised drag coefficients for each of the screens which give solutions which are consistent with the free surface wave amplitudes in the tank. Such a process is described in detail in Crowley and Porter (in press). For the small number of screens being used here, this is not an onerous numerical task. However, this implies that the solution and therefore the key properties of the solution, μ and ν, depend upon $\hat{x}$ and so (4.6) is an implicit equation for $\hat{x}$ which also has to be solved by numerical root finding.

4.4 Comparison with experimental results

First, we briefly present a comparison of our results with the recent experimental results of Faltinsen *et al.* (2011b) for a tank, unconnected to a TLD system and forced with a prescribed amplitude of motion. Thus Faltinsen *et al.* (2011b) considered a tank of aspect ratio $a/h = 1.25$ containing a single slatted screen with varying porosity and number of gaps. The tank and fitted screen were forced to oscillate with an amplitude of $\epsilon/h \approx 0.0025$ and the height of the free surface at the wall as a function of frequency in steady state (i.e. after transient decay) was recorded. As examples, figures 6 (a) and (b) display the results of
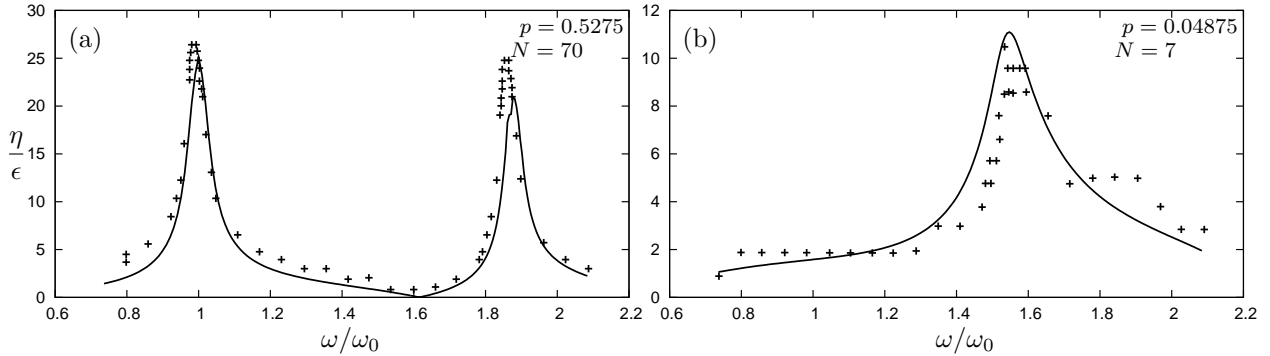
FIGURE 6: The non dimensional theoretical (solid curves) and experimental (dots) free surface wave elevations at the vertical wall, non dimensionalised by the forcing amplitude ϵ, against the forcing frequency ω which is scaled by the lowest sloshing frequency of the tank with no screens, ω_0. Forcing amplitude $\epsilon/h = 0.0025$, tank ratio $a/h = 1.25$.

our numerical model (solid curves) with the experimentally measured amplitudes (dots) for the two extreme cases of porosity considered by Faltinsen *et al.* (2011b) of $p = 0.5275$ and $p = 0.04875$ for screens with $N = 70$ and $N = 7$ gaps respectively. We see the large peaks in the response associated with tank resonances at frequencies $\omega/\omega_0 = 1$ and $\sqrt{3}$ for high porosity, and at $\omega/\omega_0 = \sqrt{2}$ for low porosity centrally-placed screens in line with comments made earlier at the end of section 2. The agreement between our model, the results of the theoretical model used by Faltinsen *et al.* (2011b) and the experiments appears to be quite good.

Now we move onto TLD systems in which we aim to determine the response $\hat{x}$ as a function of frequency. We make comparison with experimental results in Tait (2008) in order to verify our numerical results. In these model experiments the structure had mass $M = 4040\,\text{kg}$, stiffness $K = 49656\,\text{N/m}$ and a coefficient of mechanical damping $C = 14\,\text{Ns/m}$ which we supplement into our system shown in figure 4. A tank of length $2a = 0.966\,\text{m}$ and breadth $0.874\,\text{m}$ is fitted with two screens of porosity $p = 0.58$ at $a_{1,2} = \pm 0.2a$ and filled with water to a depth of $h = 0.119\,\text{m}$. We divide the structure properties M, K and C, and the external force f_e by the breadth of the tank in order to obtain quantities per unit width of the experiment to substitute into our two dimensional model. Figure 7 plots the non dimensional structural response when subject to sinusoidal excitation of amplitude $f_e = 11.7\,\text{N}$ and $f_e = 22.9\,\text{N}$ respectively. Our numerical results show excellent agreement with the experimental results in both cases.

4.5 Optimising the structural damping

Tait (2008), whose work is probably most closely connected to ours, Ostermann and Frandsen (2005) among others have all conducted scale model structure-TLD experiments. All seem to be in agreement that a typical tall structure should have a first eigenfrequency $f = \frac{1}{2\pi}\sqrt{\kappa/M} = \Omega/2\pi$ between 0.3–1Hz and, in general, the mass of the TLD should be 1–5% of the mass of the structure. Our results have been based on the following model parameters. We let the structure have mass $M = 10000\text{kg}$ and stiffness $K = 150000\text{N/m}$, each per unit length of the structure. Then $f = 0.616$Hz and the natural frequency of the structure is $\Omega = \sqrt{15}\text{s}^{-1}$. Scaling f_e appropriately from the forcing amplitudes used by Tait
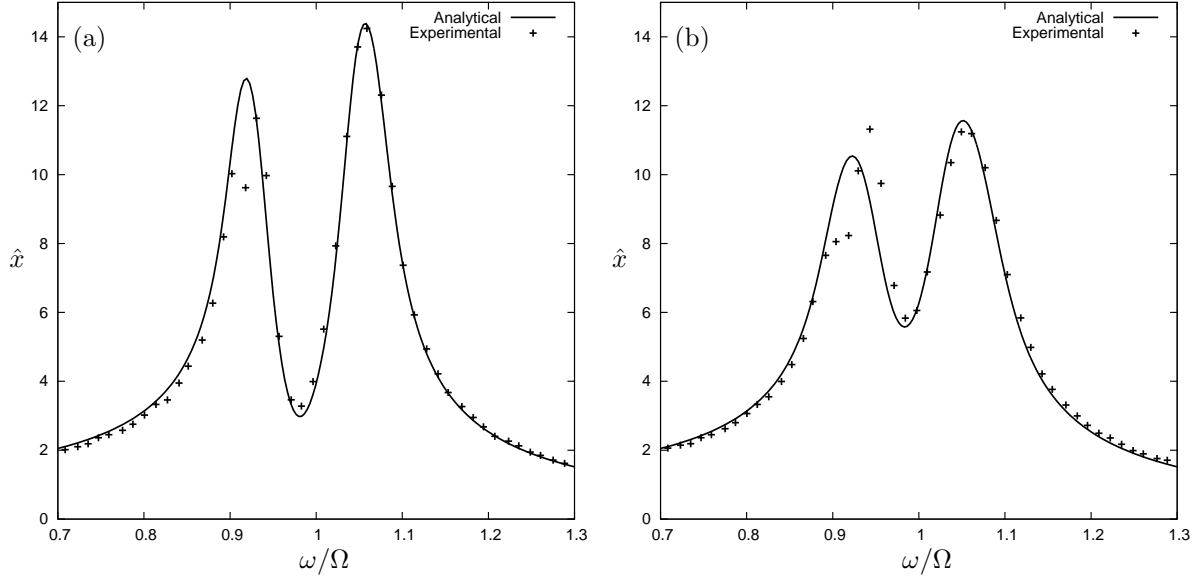
FIGURE 7: Comparison of analytical and experimental results from Tait *et al.* (2008) of the non dimensional structural response when subject to sinusoidal excitation. The TLD is of aspect ratio $a/h = 4.059$ filled to a depth of $h = 0.119\,\mathrm{m}$ and fitted with two porous screens of porosity $p = 0.58$ placed at $a_j = \pm 0.2a$. In (a) $F_e = 11.7\mathrm{N}$ and (b) $F_e = 22.9\mathrm{N}$.

(2008) based on the mass of our theoretical structure, we set $f_e = 60\mathrm{N}$ such that the forcing corresponds to expected full scale structural accelerations induced by the wind for example.

With these parameters fixed, we investigate with rectangular tanks set to have aspect ratio $a/h = 2, 3, 4$, each tuned such that the first liquid sloshing frequency in a tank with no screens is equal to the natural frequency of the structure, Ω. This process defines the size of the tank and the associated mass ratios and fluid depths for each tuned tank are listed in Table 1.

Figure 5(a) illustrates the effectiveness of a TLD. With the addition of a tank with no screens with $a/h = 3$ (the T3 configuration) the structural resonance at $\omega = \Omega$, as in (4.7), is suppressed and two new resonant frequencies are introduced either side of the original resonance, given by (4.17). The addition of a screen of porosity $p = 0.5$ in centre of the tank significantly reduces the resonant motions of the structure even when, in this case, the mass of the water in the tank is just 1.6% of the mass of the structure.

Figure 5(b) shows the structural response for a centrally placed screen in a tank with T3 configuration of $a/h = 3$ for a range of porosities, including the case $p = 0.5$ shown in figure 5(a). If the screen is too porous the tank does not provide enough of a damping force and two resonance peaks can be seen either side of $\omega = \Omega$ – as for a tank with no screens. If the screen is too solid, $\gamma \equiv \gamma_1 \to 0$, the damping becomes excessive and the sloshing fails to effectively suppress the motion of the structure at $\omega = \Omega$. For large porosities and hence small blockage and damping, the figures confirm the predictions made by the analysis at the end of §4.2. The porosity for the T3 configuration with a single screen which most effectively damps the motion (i.e. reduces the maximum response across all frequencies) of the structure is seen to be near $p = 0.5$.

In figure 5(b), the curves appear to all pass through two common points. A magnification of these areas reveal that they do not. Similar observations apply to later figures. For the
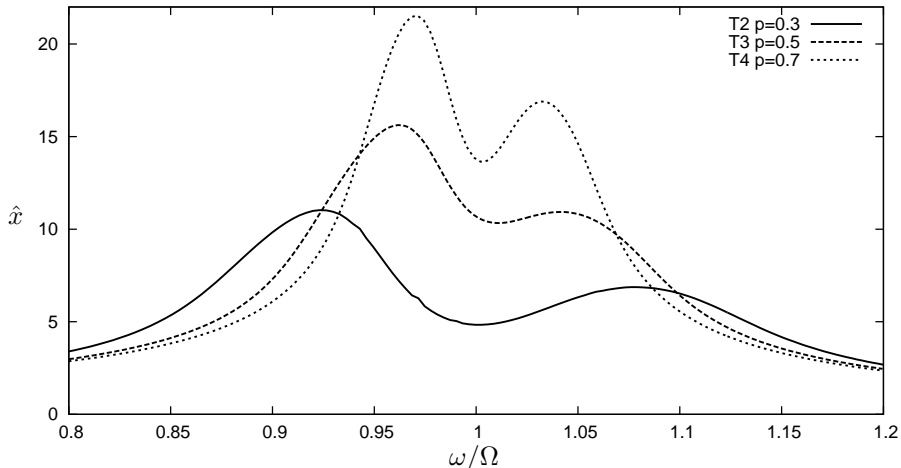
20

FIGURE 8: Non dimensional structural response $\hat{x}$ as a function of frequency for a single centrally-placed screen in a tank with TLD configuration T2, T3, T4 ($a/h = 2, 3, 4$). In each case porosity, p, chosen to give optimal damping.

related area of tuned mass dampers (TMDs), it has been shown that curves do all pass through common points (Ibrahim (2005) p.612). Perhaps it is not surprising that this is close to happening for TLDs as it is common to approximate TLDs as an equivalent TMD – see Tait (2008) and Vandiver and Mitome (1979) for example.

Similarly for the T2 ($a/h = 2$) tank configuration, the optimal porosity of a single screen is found to be near $p = 0.4$, whilst for the wider T4 ($a/h = 4$) tank, a porosity close to $p = 0.5$ is found to be optimal. For each of the three configurations with a single screen, the optimal parameters of porosity are used to compare the response in figure 8. Unsurprisingly the results show that the larger the mass ratio, $\hat{m}$, the better the damping performance. From a practical perspective, one would have to balance the economic cost of a larger fluid mass with the enhanced damping it provides.

The next question to address is whether we can improve the TLD efficiency through both the choice of tank geometry and the number and placement of screens. For tank configurations T3 and T4, we have considered screens of porosity $p = 0.3, 0.4, 0.5$ and 0.6 and $p = 0.5, 0.6, 0.7$ and 0.8 respectively. For each value of p we wish to optimise the position of the screens in the tank in order to minimise the structural response. Table 2 lists the five chosen initial screen locations in this process. Screens of porosity greater than 0.8 are not considered as larger number of them would be required in order to gain the required amount of inherent damping in the tank. Similarly for more impervious screens with $p < 0.3$, the number of screen locations to obtain minimum structural displacement would be limited.

In figure 9 each screen configuration provides a different amount of damping. When $p = 0.3$ (small porosity) the favoured configuration is case C (two screens at $\pm 0.7a$). Here the tendency is to over damp if there are too many screens or they are placed centrally where the fluid motion is largest. Increasing the porosity to $p = 0.4$, again case C is seen to provide the best overall damping. When p is increased to 0.5, case C shows slight under-damping, and now case A (one screen) shows the best overall damping. As p is increased further still to 0.6, all configurations apart from case B (two screens at $\pm 0.2a$) and case E (four screens) show varying amounts of under-damping. In general, then, we see that moving the screens towards the centre of the tank, or increasing the number of screens in the tank increases the
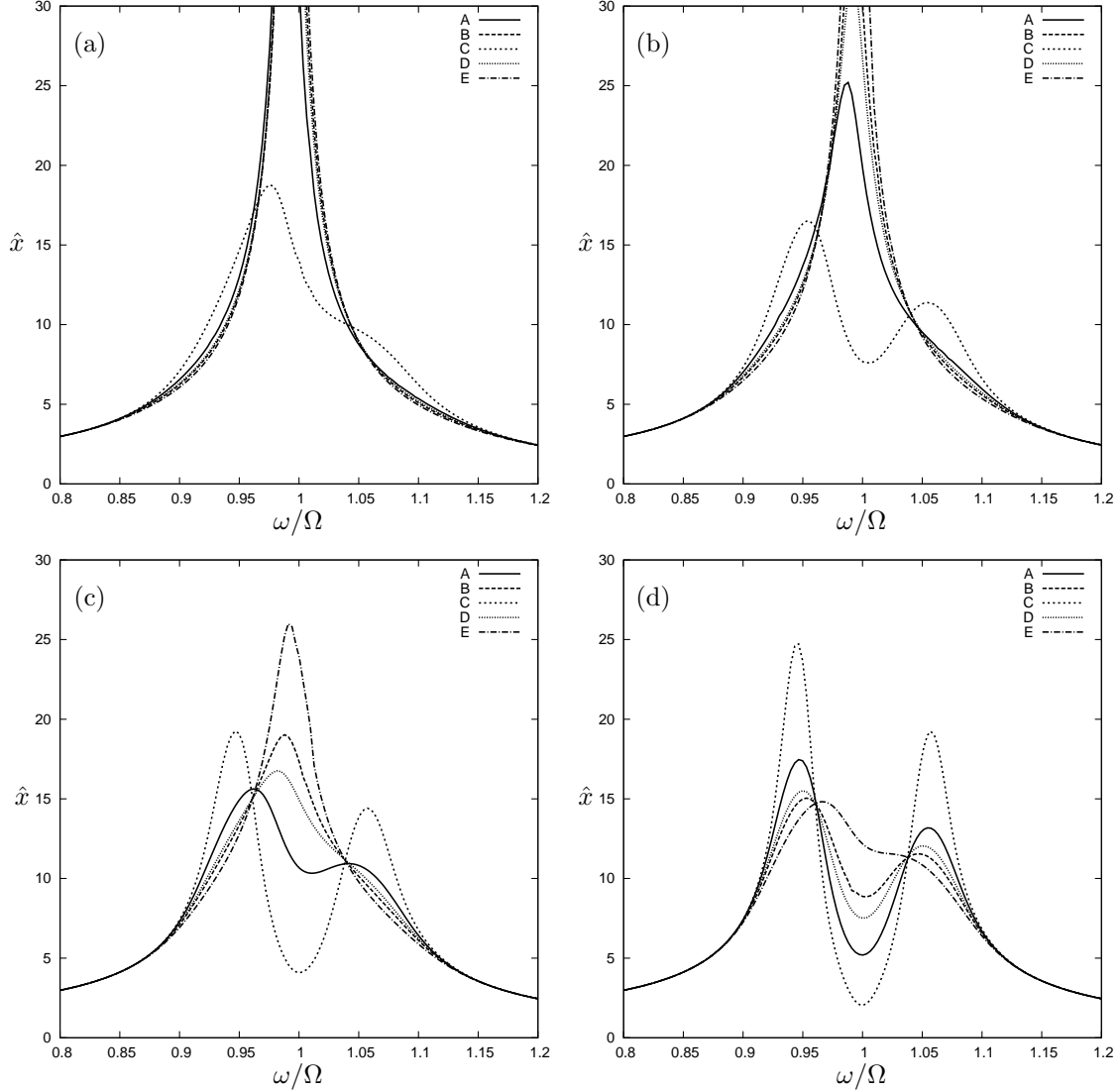
21

FIGURE 9: Non dimensional structure displacement $\hat{x}$ with TLD T3, in (a) screen porosity $p = 0.3$, (b) $p = 0.4$, (c) $p = 0.5$ and (d) $p = 0.6$.

inherent damping of the tank and vice versa.

We can use the fact that curves all appear to pass close to two common points, for each fixed p, to fine tune the damping process. Thus, an ideal screen configuration would have a curve which peaked at these two points. This fine tuning process is illustrated in figure 10 for the cases considered in figures 9(a), (b) and (d), with the configurations listed in table 3. Thus figure 10(a) uses case E as a reference curve and shows how case C with screens located at $\pm 0.7a$ can be improved by placing them slightly further apart at $\pm 0.75a$ to attain more optimum damping. Similarly in 10(b) case E is used for reference. Case A, a central screen has no flexibility in its placement, but the case C spacing of $\pm 0.7a$ can again be optimised and the spacing $\pm 0.65a$ does this. For a screen of porosity $p = 0.6$, we find that adapting case B and moving both of the screens to a more centralised position is insufficient in increasing the inherent damping of the tank. However, in figure 10(c) we show that altering case D (three screens) and moving the outer screens from $a_{1,3} = \pm 0.5a$ to $a_{1,3} = \pm 0.3a$, case I,
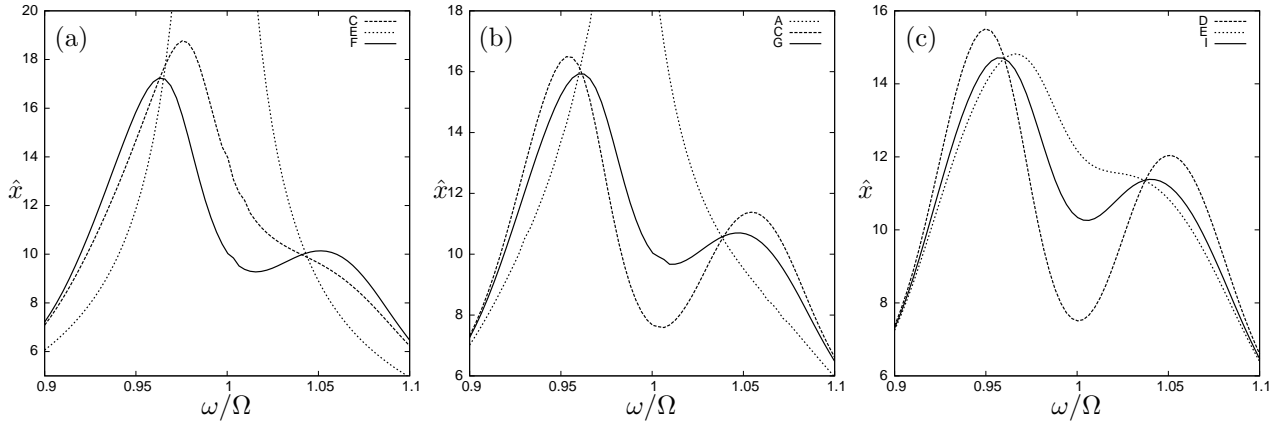
22

FIGURE 10: Non dimensional structure displacement $\hat{x}$ with TLD T3, after further optimisation of the screen locations. In panel (a) screen porosity $p = 0.3$, (b) $p = 0.4$, (c) $p = 0.6$.

results in a more optimal structural response.

We observe that the double peaks are not of equal height. It is possible to re-balance these by offsetting the tuning of the TLD frequency from the structural frequency. This has little effect on the optimal screen placements and we do not consider that level of detail here.

The same process is repeated for TLD configuration T4 and results are illustrated in figure 11 with a further optimisation of the cases $p = 0.5$, $p = 0.6$ and $p = 0.8$ shown in figure 12. For this wider tank, the general trends seen for the T3 configuration are repeated. Thus for $p = 0.5$ two screens positioned at $\pm 0.75a$ (case F, adapted from case C) are found to be optimal. Case G (adapted from case C) is optimal for $p = 0.6$, and then case K (four screens adapted from case E) is optimal for the highest porosity considered, $p = 0.8$. Details of the further optimised screen configurations are given in table 3.

Once the optimal screen arrangements for screens of given porosity in the restricted range have been chosen, the magnitude of the structural displacement for each of these two TLD arrangements can be compared. From figure 13, for both tank configurations T3 and T4, it appears that the only significant distinguishing feature between these optimised cases is the relative height of the double peaks. As mentioned previously TLDs are often best designed such that these peaks are of equal height which, for this test structure, is best achieved with screens of porosity $p = 0.6$ and $p = 0.8$ in screen locations I (three screens) and K (four screens) for tank configurations T3 and T4 respectively.

Thus, in the process of designing a TLD for a particular structure, given a screen where the porosity known, the optimal arrangement and number, N, of these screens could be chosen in order to minimise the structural displacement when under horizontal excitation. The tank size would be determined by space limitations and liquid depth set in order to tune the sloshing frequency of the tank to the natural frequency of the structure. Alternatively, if a porous screen could be designed of any required permeability, then for simplicity it would make sense to construct a TLD with just one screen in the centre of the tank - with screen porosity optimised accordingly.
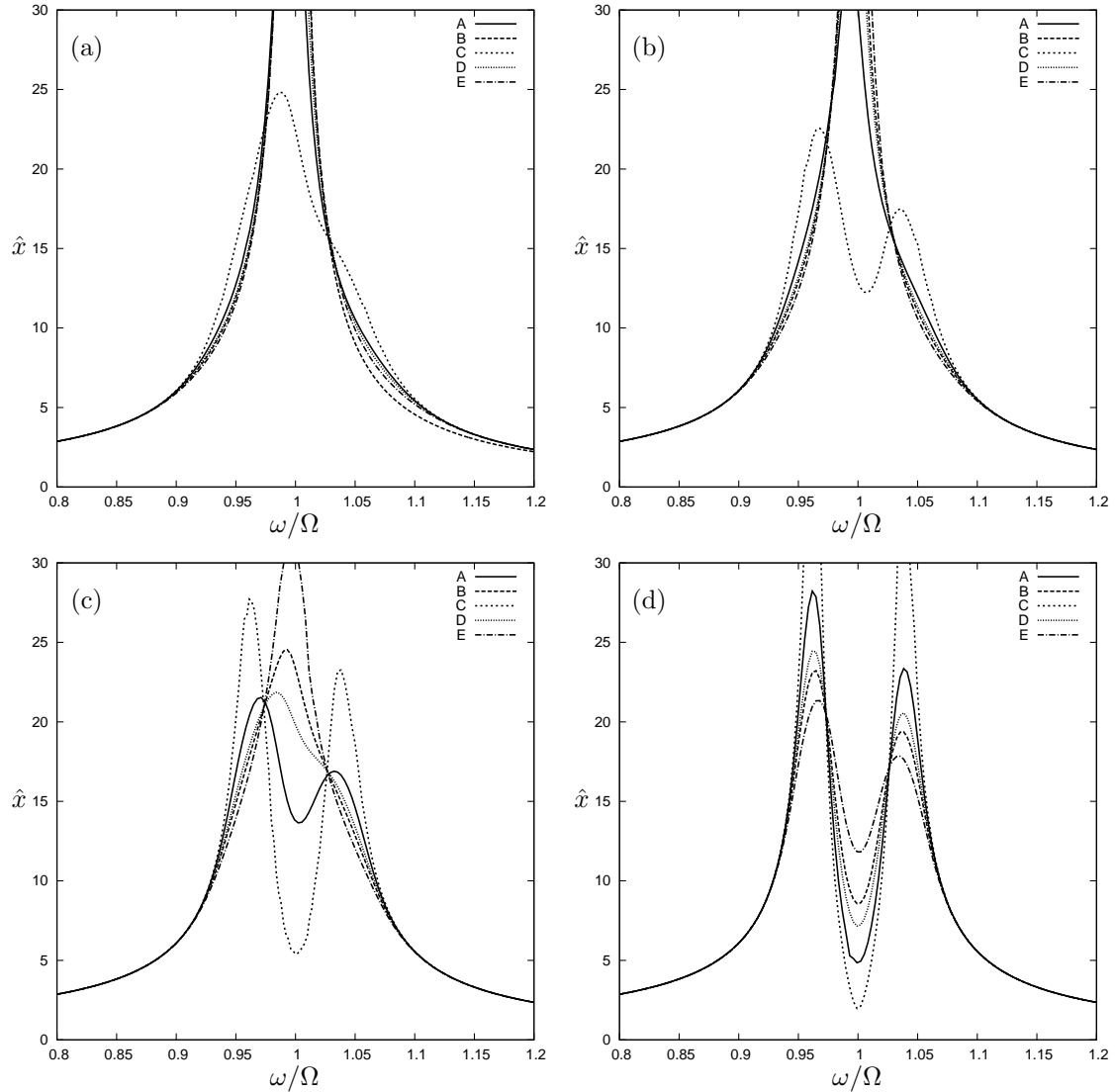
FIGURE 11: Non dimensional structure displacement $\hat{x}$ with TLD T4, in (a) screen porosity $p = 0.5$, (b) $p = 0.6$, (c) $p = 0.7$ and (d) $p = 0.8$.

5 Conclusions

In this paper we have considered a two-dimensional tuned liquid damper system consisting of a liquid-filled rectangular tank fitted with vertical slatted screens mounted on a mechanical mass/spring system. The mathematical model that has been derived for forced liquid sloshing gives simple exact solutions to a linear water wave problem in which a novel realistic screen-averaged linear condition has been used for the slatted screen. Linearisation is the key to producing a solution which can be expressed simply comprised in terms of a system of 2×2 transfer matrices in each of the depth modes in the tank and applicable to any number of screens. We have illustrated the key features of tuned liquid dampers explicitly using the mathematical solutions that have been derived. Furthermore, numerical results produced via this method to calculate the structural response show good agreement when compared to existing experimental results.
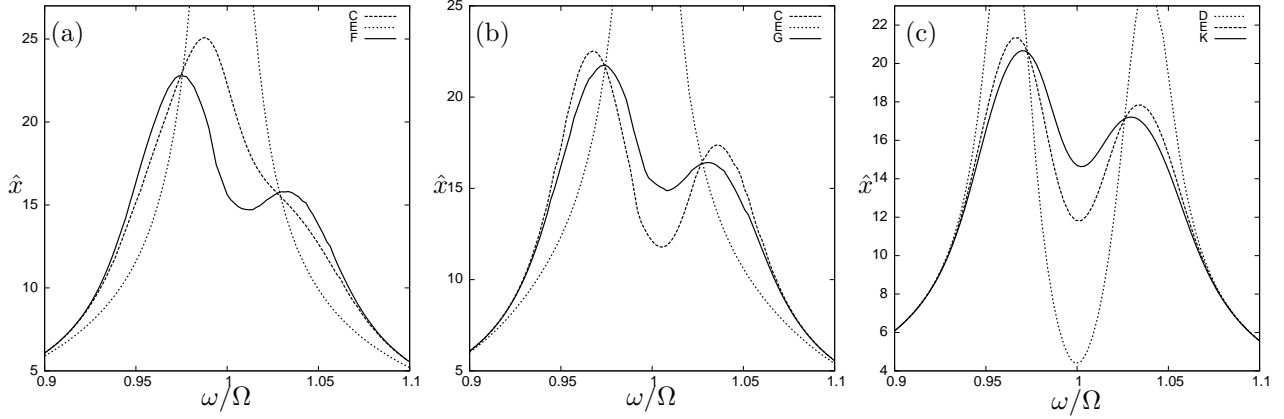
FIGURE 12: Non dimensional structure displacement $\hat{x}$ with TLD T4 after further optimisation of screen placement. In panel (a) screen porosity $p = 0.5$, (b) $p = 0.6$, (c) $p = 0.8$.

Tank size	Porosity	Configuration	Number of screens	Locations
$T3$	0.3	F	2	$\pm 0.75a$
	0.4	G	2	$\pm 0.65a$
	0.5	H	3	$\pm 0.65a$, 0
	0.6	I	3	$\pm 0.3a$, 0
$T4$	0.5	F	2	$\pm 0.75a$
	0.6	G	2	$\pm 0.65a$
	0.7	J	3	$\pm 0.6a$, 0
	0.8	K	4	$\pm 0.2a$, $\pm 0.4a$

TABLE 3: Near optimal configurations of both the number of screens and their location for tanks $T3$ and $T4$ with screens of a prescribed porosity.

The ultimate goal of this investigation has been to determine optimal configurations of screens including the number and position of the screen within the tank and well as the porosity of the screen. The model has been applied to three prototype tank configurations to illustrate that optimal screen configurations depend on the system being considered (in particular the structure/liquid mass ratio and the tank aspect ratio). In the two configurations considered in detail in the results, the optimal strategy involved either two or four screens placed in the tank at specific locations and having relatively high porosity, illustrating that the need to use a model such as this to produce an optimal design of tuned liquid damper in practical applications.

References

Abramson, H. (1966). The Dynamic Behavior of Liquids in Moving Containers. NASA SP-106. *NASA Special Publication 106*.

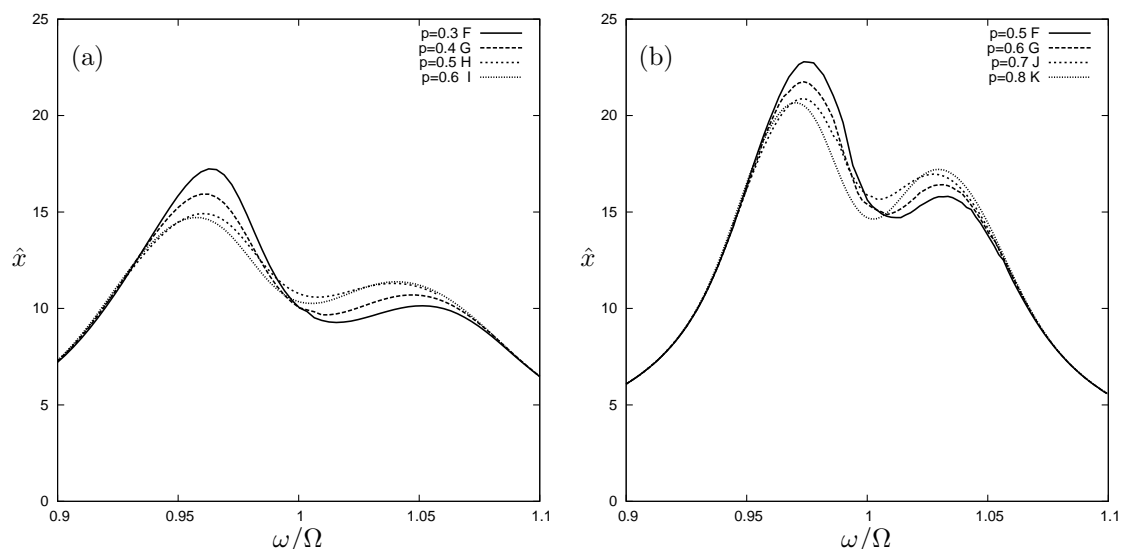Abramson, H., W. Chu, and L. Garza (1963). Liquid sloshing in spherical tanks. *AIAA*

FIGURE 13: The structure-frequency response when coupled with TLD (a) T3 and (b) T4 with 'optimised' screen locations for screens of porosity $p = 0.3 - 0.8$.

J 1(2), 384–389.

Bennett, G., P. McIver, and J. Smallman (1992). A mathematical model of a slotted wave-screen breakwater. *Coastal engineering 18*(3-4), 231–249.

Crowley, S. and R. Porter. The effect of slatted screens on waves. *Journal of Engineering Mathematics*, Preprint available from http://www.maths.bris.ac.uk/ marp/abstracts/slatted–screen.pdf.

Dodge, F. (2000). The New "Dynamic Behavior of Liquids in Moving Container". *Southwest Research Institute, San Antonio, Texas*.

Evans, D. (1990). The use of porous screens as wave dampers in narrow wave tanks. *Journal of Engineering Mathematics 24*(3), 203–212.

Faltinsen, O., R. Firoozkoohi, and A. Timokha (2011a). Analytical modeling of liquid sloshing in a two-dimensional rectangular tank with a slat screen. *Journal of Engineering Mathematics 70*, 93–109.

Faltinsen, O., R. Firoozkoohi, and A. Timokha (2011b). Steady-state liquid sloshing in a rectangular tank with a slat-type screen in the middle: Quasilinear modal analysis and experiments. *Physics of Fluids 23*, Art. no. 042101.

Faltinsen, O. and A. Timokha (2011). Natural sloshing frequencies and modes in a rectangular tank with a slat-type screen. *Journal of Sound and Vibration 330*, 1490–1503.

Fediw, A., N. Isyumov, and B. Vickery (1995). Performance of a tuned sloshing water damper. *Journal of wind engineering and industrial aerodynamics 57*(2-3), 237–247.

Frandsen, J. (2005). Numerical predictions of tuned liquid tank structural systems. *Journal of fluids and structures 20*(3), 309–329.

Gardarsson, S., H. Yeh, and D. Reed (2001). Behavior of sloped-bottom tuned liquid dampers. *Journal of Engineering Mechanics 127*, 266.

Ibrahim, R. (2005). *Liquid sloshing dynamics: theory and applications.* Cambridge Univ Pr.

Kareem, A., T. Kijewski, and Y. Tamura (1999). Mitigation of motions of tall buildings with specific examples of recent applications. *Wind and Structures 2*(3), 201–251.

Kronig, R. (1926). On the theory of dispersion of x-rays. *JOSA 12*(6), 547–556.

Love, J. and M. Tait (2010). Nonlinear simulation of a tuned liquid damper with damping screens using a modal expansion technique. *Journal of Fluids and Structures.*

Martin, P. (2006). *Multiple scattering: interaction of time-harmonic waves with N obstacles,* Volume 107. Cambridge Univ Pr.

Mei, C., M. Stiassnie, and K. Dick (1983). *Theory and applications of ocean surface waves.* World Scientific.

Tait, M. (2008). Modelling and preliminary design of a structure-TLD system. *Engineering Structures 30*(10), 2644–2655.

Tait, M. and A. El Damatty (2004). Testing of tuned liquid damper with screens and development of equivalent TMD model. *Wind & Struct. 7*(4), 215–234.

Tait, M., A. El Damatty, N. Isyumov, and M. Siddique (2005). Numerical flow models to simulate tuned liquid dampers (TLD) with slat screens. *Journal of Fluids and Structures 20*(8), 1007–1023.

Tamura, Y., K. Fujii, T. Ohtsuki, T. Wakahara, and R. Kohsaka (1995). Effectiveness of tuned liquid dampers under wind excitation. *Engineering structures 17*(9), 609–621.

Tamura, Y., R. Kousaka, and V. Modi (1992). Practical application of nutation damper for suppressing wind-induced vibrations of airport towers. *Journal of Wind Engineering and Industrial Aerodynamics 43*(1-3), 1919–1930.

Vandiver, J. and S. Mitome (1979). Effect of liquid storage tanks on the dynamic response of offshore platforms. *Applied Ocean Research 1*(2), 67–74.

Warnitchai, P. and T. Pinkaew (1998). Modelling of liquid sloshing in rectangular tanks with flow-dampening devices. *Engineering Structures 20*(7), 593–600.